

On tidal array layout sensitivity to regional hydrodynamics representation

Connor Jordan, Daniel S. Coles, Fraser Johnson and Athanasios Angeloudis

Abstract—In-stream tidal devices are ready to be deployed, yet the largest operational commercial array is limited to 6MW. Upcoming government support should see the size of such arrays increase by orders of magnitude, and thus the optimal placement of turbines within tidal arrays is an emerging challenge for successful commercial integration. Hydrodynamic models are required to predict the power produced by an array and the impact on the surrounding environment. The influence of common model inputs to layout optimisation are investigated herein. This is achieved using a shallow water equation based tidal array modelling framework, *Thetis*, coupled with a low cost analytical wake model (*FLORIS*) that allows for rapid assessment of the impact of small changes in hydrodynamic results on array micro-siting. The sensitivity of array optimisation at an intermediate development point (43 turbines) is interrogated through both artificial flow field manipulation and the variation of model input pertinent to the optimisation. A small margin exists in which an optimised array layout will perform efficiently for a deviation in flow prediction accuracy. However, incorrect flow predictions by a range sensitive to model inputs had a reduction of almost 8% on array efficiency relative to a control case. The sensitivity of flow field variance by model input changes, on extractable energy and array layout are substantial. Comparing arrays sited on flow fields using different bathymetry resolution leads to a discrepancy on average of over 2% to average array power. Arrays sited for different mesh resolution and friction representation also see average changes up to and exceeding 0.75%. For array developers and the future of this nascent industry, re-calibration of the model at every stage of data collection coupled with early acquisition of bathymetry data is critical not just for accurate power quantification, but also array efficiency. At a regional scale, quantification of the potential tidal resource must consider the consequences of uncertainty in model input data and site constraints that cannot yet be accounted for.

Index Terms—Tidal stream energy, tidal array micro-siting, optimisation sensitivity

© 2023 European Wave and Tidal Energy Conference. This paper has been subjected to single-blind peer review.

C. Jordan acknowledges the support of an EPSRC PhD studentship. D. Coles acknowledges the financial support of the Tidal Stream Industry Energiser project (TIGER), which is co-financed by the European Regional Development Fund through the Interreg France (Channel) England Programme. A. Angeloudis acknowledges the support of the support of the EC H2020 ILIAD DTO project under grant agreement 101037643.

C. Jordan is at the School of Engineering at the University of Edinburgh, and within the Institute for Infrastructure and the Environment, Edinburgh, UK, EH9 3FG (e-mail: c.jordan@ed.ac.uk)

D. Coles is at the School of Engineering, Computing and Mathematics at the University of Plymouth, Drake Circus, Plymouth, PL4 8AA (e-mail: daniel.coles@plymouth.ac.uk)

F. Johnson is the Operations and Maintenance Manager on the Meygen project for SIMEC Atlantis Energy Ltd (e-mail: fraser.johnson@saerenewables.com)

A. Angeloudis is at the School of Engineering at the University of Edinburgh, and within the Institute for Infrastructure and the Environment, Edinburgh, UK, EH9 3FG (e-mail: a.angeloudis@ed.ac.uk).

Digital Object Identifier:
<https://doi.org/10.36688/ewtec-2023-302>

I. INTRODUCTION

SEVERAL configurations of in-stream tidal devices exist, waiting to be deployed at sea to convert much needed renewable energy from the currents. In spite of the available commercial options, there are limited numbers of turbines operating in the ocean, with the largest operating array currently capped at 6MW. A figure often cited is the 11% of UK electricity demands that tidal energy could satisfy [1], but the accuracy of this claim is challenged as investigations into resource assessment improvements continue. Whilst many mechanisms to achieve levelised cost of energy (LCOE) reductions are available [2], few are as critical in the sustainability of this nascent industry as array layout – both for resource assessment and scheme development.

To assess array layout and to maximize the power output, the surrounding region needs to be modelled to accurately capture the governing hydrodynamics. A well-renowned, workable method of encapsulating a region on the scale of 10-100 kilometres is by implementing 2D or 3D hydrodynamic models, based on the shallow water equations (SWEs). In these models, individual turbines can be represented as momentum sinks at discrete locations, accommodating basic wake modelling and prediction of array power. However, once turbine representation is depth-averaged and simplified to a discrete patch of increased drag, the designer may lose focus of the constraints that the device may entail. On the other hand, too much focus on such constraints may neglect consideration of the uncertainty in the model used to design the array.

Various estimates have been reported on the extractable energy at sites such as the Inner Sound of the Pentland Firth, UK, with significant variation based on modelling methods and data availability. Numerous optimisation techniques [3]–[6] have been developed for array micro-siting but where applied practically, these studies do not quantify the difference in potential power production as a result of the data used to represent the regional hydrodynamics. This work will utilise the methodology of [7] where an analytical wake model designed for wind array operation and optimisation (*FLORIS* from the US National Renewable Energy Laboratory) was adapted for use in conjunction with a coastal ocean model (*Thetis*). A greedy optimisation algorithm will be applied for varying cases of a prospective site for array expansion (i.e. the Inner Sound) with practical limits on placement based on energy yield and minimum separation. The optimisation strategy will be employed to emphasise

sensitivities in micro-siting that may have a substantial impact on the implementation of tidal arrays.

II. METHODOLOGY

A. Hydrodynamic modelling

*Thetis*¹, is employed for hydrodynamic modelling, utilising *Firedrake* [8], [9] to solve associated partial differential equations using finite elements. *Thetis* is used in its 2D configuration, solving the non-conservative form of the non-linear shallow-water equations,

$$\frac{\partial \eta}{\partial t} + \nabla \cdot (H_d \mathbf{u}) = 0, \quad (1)$$

$$\frac{\partial \mathbf{u}}{\partial t} + \mathbf{u} \cdot \nabla \mathbf{u} + g \nabla \eta = \nabla \cdot (\nu (\nabla \mathbf{u} + \nabla \mathbf{u}^T)) - \frac{\tau_b}{\rho H_d} - \frac{c_t}{\rho H} |\mathbf{u}| \mathbf{u} + f \mathbf{u}^\perp, \quad (2)$$

where η is the water elevation, H_d is the total water depth, \mathbf{u} is the depth-averaged velocity vector, and ν is the kinematic viscosity of the fluid. The term $f \mathbf{u}^\perp$ represents the Coriolis “force”, \mathbf{u}^\perp is the velocity vector rotated counter-clockwise over 90° , and $f = 2\Omega \sin(\zeta)$ with Ω the angular frequency of the Earth’s rotation and ζ the latitude. The bed shear-stress (τ_b) effects are represented through the Manning’s n_M formulation as per [10]:

$$\frac{\tau_b}{\rho} = g n_M^2 \frac{|\mathbf{u}| \mathbf{u}}{H_d^{\frac{1}{3}}}, \quad (3)$$

The treatment of inter-tidal processes, discretisation and time-marching are covered in [7]. The thrust coefficient, c_t , corresponds to a momentum sink for the presence of the turbines and is discussed both in [7] and Section II-B.

B. Tidal array modelling

The force applied by the tidal array when represented using the linear momentum actuator disc theory is:

$$F_{\text{array}} = \frac{1}{2} \int_{\Omega_{\text{array}}} \rho c_t(\mathbf{x}) |\mathbf{u}(\mathbf{x})| \mathbf{u}(\mathbf{x}) d\mathbf{x}, \quad (4)$$

with the thrust coefficient, $c_t(\mathbf{x})$, defined as:

$$c_t(\mathbf{x}) = C_t(\mathbf{u}(\mathbf{x})) A_t d(\mathbf{x}), \quad (5)$$

where A_t is the turbine swept area, C_t is the thrust coefficient as a function of the velocity $\mathbf{u}(\mathbf{x})$, and $d(\mathbf{x})$ is the local turbine density [7]. Thus, following the notation of (4), the power extracted at any given moment by the array can be approximated as

$$P_{\text{array}} = \frac{1}{2} \int_{\Omega_{\text{array}}} \rho c_p(\mathbf{x}) |\mathbf{u}(\mathbf{x})|^3 d\mathbf{x}, \quad (6)$$

where $c_p(x)$ is a power coefficient function given as

$$c_p(\mathbf{x}) = C_p(\mathbf{u}(\mathbf{x})) A_t d(\mathbf{x}), \quad (7)$$

and C_p is a power coefficient as per [7].

C. Analytical wake model

FLORIS is utilised as the analytical wake model for the optimisation process, with a Gaussian description of the wake [11];

$$\frac{\Delta U}{U_\infty} = \left(1 - \sqrt{1 - \frac{C_T}{8(k^* x/d_0 + \epsilon)^2}} \right) \times e^{\left(-\frac{1}{2(k^* x/d_0 + \epsilon)^2} \left\{ \left(\frac{z - z_h}{d_0} \right)^2 + \left(\frac{y}{d_0} \right)^2 \right\} \right)} \quad (8)$$

where U_∞ is the approaching streamwise velocity, z is the wall-normal coordinate with z_h the turbine hub height, k^* is the growth rate of the wake ($\partial \sigma / \partial x$), d_0 is the diameter of the turbine and ϵ is the normalised Gaussian velocity deficit at the rotor plane. The local wake growth rate k^* is estimated using the local streamwise turbulence intensity, \mathcal{I} [12]. Free-stream linear superposition is applied as in [7].

D. Optimisation methodology

The custom greedy algorithm of [7] is adopted. Greedy algorithms allow straightforward masking processes for placement restriction such as enforcing minimum spacing constraints. As this approach places one turbine at a time, the optimisation parameters considered in the micro-siting algorithm (i.e. x- and y- turbine coordinates) are constrained relative to conventional approaches allowing for quick assessment of arrays extending to hundreds of turbines.

Some minor differences in application are made relative to [7]:

- When *FLORIS* identifies the location in the domain with the highest velocity and adds a turbine, this is now done using the hub-height flow map to save computational time in depth-averaging flow fields at different planes.
- The approach to selecting ambient flow fields is the same as [7], but using just four flow fields in total for ebb and flood directions.
- The performance constraints are optimised for each case to deal with variation in flow speed across the flow fields. See Table I. The minimum separation constraint is consistent at 1.5 diameters.

E. Site: Inner Sound, Pentland Firth

The Meygen project² is situated in the Inner Sound of the Pentland Firth along the coast of north east Scotland. Alongside the Orkney archipelagos, this area experiences the magnitude of flow required to generate substantial power for the UK energy grid. Tidal open boundaries are forced using the Q1, O1, P1, K1, N2, M2, S2 & K2 tidal constituents from TPXO [13] and the model is run initially with 2 days of spin up time. To generate flow fields for optimisation, the model is run for 30 days and appropriate snapshots are selected. In total, there are 8 sensitivity cases outlined in Section II-F generated by varying input data. When assessing power in *Thetis* of array layouts sited for these cases, the model is run for 10 days to include peak spring

¹<http://thetisproject.org/>

²<https://saerenewables.com/tidal-stream/meygen/>

and ebb tides. Two meshes are employed for these cases, alongside varying levels of bathymetry data and bed friction. The baseline mesh is the one used in [7], with Fig. 1 showing the primary location of mesh refinement indicating the siting limits and the area where additional bathymetry data is available. The original mesh with a variable friction field and lower resolution bathymetry (later denoted as Case OM-LR-VF) was previously validated to acceptable accuracy for methodological demonstrations as presented in [7] and thus the same calibration parameters are adopted.

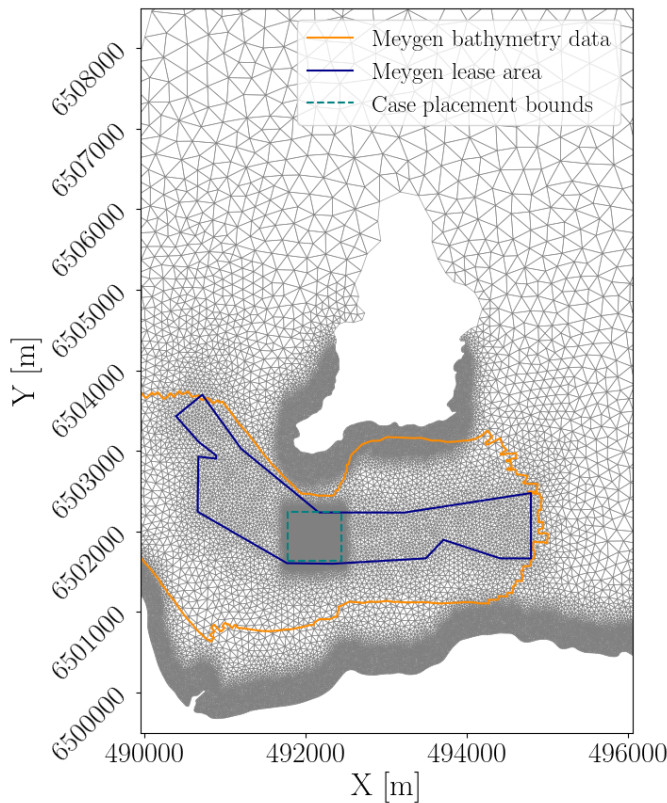


Fig. 1. Refined computational mesh around Stroma and north east Scotland plotted using UTM Zone 30N. The boundaries of the additional high-resolution Meygen bathymetry area, Meygen lease area and placement boundaries for the cases considered are shown. For comparison to the original mesh refer to [7].

Key model component differences between the study setups can be summarised as follows:

1) *Meshing*: The original mesh (OM) is identical to that of [7] with element size varying from 300–1,500m close to islands and the shoreline up to 20,000m at the seaward boundaries. At the Meygen site, the mesh is refined to a 5m element size corresponding to $\approx \frac{1}{2}$ blade length. For sensitivity analyses, a refined mesh (RM) is resolved to 20m on the lower half of Stroma and at the North East tip of the mainland to account for more accurate coastlines. The mesh generation process includes defining multiple rasters to accommodate this higher resolution of boundaries near the array area based on higher resolution data that was not included in [7].

2) *Bed shear stress*: In the absence of accurate bed classification data, a constant bed friction coefficient (CF) is often assumed. The influence of this assumption is explored with variable friction fields (VF) derived by data obtained from the British Geological Survey [14].

3) *Bathymetry*: Finally, bathymetry data in [7] was provided by the Edina Digimap Service [15] (LR). Data collected for the Meygen project (HR) has been made available to the scale of 0.2m, which has been interpolated to a 0.5m grid based on the element resolution used within the array area.

F. Sensitivity case studies

To determine the influence of common model input fields 8 cases are generated in *Thetis* by varying the friction representation, bathymetry dataset combination and mesh. A summary of the cases is presented in Table I. The velocity magnitude and direction is measured at the locations of two Acoustic Doppler Current Profilers (ADCPs - one for ebb, one for flood, as per [7]) in order to determine the variation between various models and measured data at these points. Case RM-HR-VF is selected to be a baseline case for comparison as it includes the most data from the Meygen site. The difference in velocity magnitude and principal direction for each of the 8 cases and reality at the ADCP locations are then calculated. This provides a range of values to artificially modify baseline case velocity fields by, subsequently re-siting arrays to indicate the sensitivity of layout micro-siting to uniform changes of the flow fields. Following this, the influence of input data on the device layout configuration is investigated by independently optimising and testing the layouts on each case through an inter-comparison.

1) *Sensitivity to flow field magnitude and direction deviation*: Velocity magnitude and direction are artificially modified in *FLORIS*, to assess sensitivity to the values ranges observed between models in *Thetis* (Table III). The magnitude is incrementally varied and the direction is uniformly rotated. Whilst unrealistic, a uniform variation exercise provides an intuitive basis of understanding the influence of uncertainty of the input data may have on the optimisation results. Performance based constraint parameters outlined in [7] are employed to ensure productive micro-siting, based on individual turbine power performance reductions, A , cumulative individual power performance reductions, B , and snapshot capacity factor, Γ . For the investigation into uniform changes in flow, all optimisations are performed with $A = 0.10$, $B = 0.175$ and $\Gamma = 0.50$.

2) *Sensitivity to model input changes*: Each simulation case generates a non-uniform change in flow pattern across the optimisation region. An array is micro-sited for each case and its resultant power quantified for all other cases i.e. each of the 8 optimised arrays are simulated for all input combinations. The choice of flow fields are consistent, but display variation in field average magnitude which impacts the efficiency of the optimisation with the initial performance constraint parameters outlined above. As only 4 flow fields are used, the performance constraint parameters must react to the change in flow field, for example the snapshot capacity factor should be reduced if the velocity is lower across the optimisation space. Updated parameters are presented in Table I.

TABLE I
PENTLAND FIRTH CASE VARIANCES. THE BASELINE CASE FOR INITIAL INVESTIGATIONS FOR UNIFORM CHANGES TO THE FLOW FIELD IS HIGHLIGHTED IN BOLD.

Case ID	Mesh	Bathymetry	Bed friction	Min. average snapshot utilisation ratio, Γ	Max. single turbine power reduction, A	Max. cumulative single turbine power reduction, B
OM-LR-CF	Original	Low res.	Constant	0.50	0.10	0.175
OM-LR-VF	Original	Low res.	Variable	0.40	0.15	0.25
OM-HR-CF	Original	High res.	Constant	0.50	0.10	0.175
OM-HR-VF	Original	High res.	Variable	0.40	0.125	0.20
RM-LR-CF	Refined	Low res.	Constant	0.50	0.10	0.175
RM-LR-VF	Refined	Low res.	Variable	0.40	0.15	0.25
RM-HR-CF	Refined	High res.	Constant	0.50	0.10	0.175
RM-HR-VF	Refined	High res.	Variable	0.50	0.10	0.175

3) *Sensitivity to support structure inclusion*: One feature that may be overlooked in depth-averaged models is the support structure as it cannot be modelled independently from the rotors unless further resolution is provided. Notably in [7] (and for the sensitivity analyses above), the support structure is not included in the formulation of the drag coefficient. However, an increase in drag will cause a larger increase in channel resistance which becomes critical as the number of turbines increases [16].

The support structure is first implemented in *Thetis* by using additional terms A_{sup} and C_{sup} which yields a revised thrust coefficient formulation of:

$$c_t(\mathbf{x}) = (C_t(\mathbf{u}(\mathbf{x})) A_t + C_{sup} A_{sup}) d(\mathbf{x}), \quad (9)$$

Where a column width and height of 2.6m and 14m are assumed respectively for the turbine support structure and thus a cross-sectional area $A_{sup} = 36.4m^2$. A drag coefficient, $C_{sup} = 0.7$ is used as per [17]. The thrust coefficients on the overall turbine are updated and the wake geometry parameters k_a , k_b , α and β are re-calibrated against a *Thetis* wake as in [7]. The updated parameters are shown in Table II.

TABLE II
CALIBRATED WAKE PARAMETERS FOR GAUSSIAN MODEL, WITH AND WITHOUT SUPPORT STRUCTURE (SS) INCLUDED IN *Thetis*.

	AR2000-20m - no SS [7]	AR2000-20m
k_a	0.1087	0.002173
k_b	0.006912	0.02272
α	0.4886	0.5751
β	0.2496	0.2974

In order to determine the influence of the support structure at small-medium array scales i.e. for an intermediate stage of the Meygen project, optimisation is re-performed on Case RM-HR-VF for 43 turbines.

III. RESULTS

Fig. 2 presents the velocity exceedance probability between 8 cases for the flood ADCP (duration of the flood only) and ebb ADCP (duration of the ebb only). As phase is tertiary in optimisation, velocity exceedance is used to provide the indication in similarity between modelled and measured data. Generally, the models correlate well except for discrepancies in velocity prediction in the flood at measured sites. The

worst case R^2 value in the ebb is 0.938 for Case RM-HR-VF, compared to flood R^2 values of 0.777 and 0.815 for Cases OM-HR-CF and RM-HR-CF respectively. Considering a single point, the mesh appears to have the least influence on velocity magnitude, whilst generally, the friction parameterisation causes the most significant change in magnitude. Variable friction cases correlate most closely in the flood, but correlate less closely to the measured data compared with constant friction cases. The introduction of the high resolution bathymetry causes increased speeds across all cases.

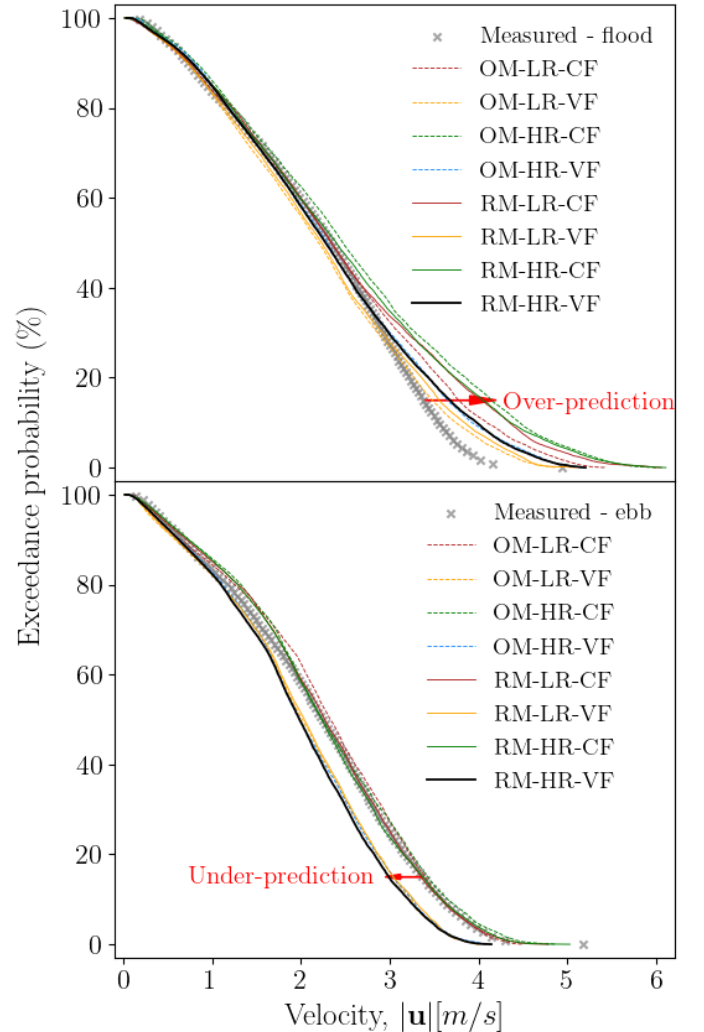


Fig. 2. Velocity exceedance plots for (a) ADCP 1 (flood) and (b) ADCP 2 (ebb) against modelled values.

TABLE III
FLOW FIELD SENSITIVITY

	Case RM-HR-VF	Measured	Minimum	Maximum	Δ_{\max}
Dominant flood direction ($^{\circ}$)	123.28	121.41	121.41	125.21	3.80
Flood velocity, u_{mean} (m/s)	2.321	2.235	2.209	2.563	0.354
Dominant ebb direction ($^{\circ}$)	279.41	271.47	271.47	279.97	8.50
Ebb velocity, u_{mean} (m/s)	1.963	2.192	1.963	2.259	0.296

Table III presents the flood and ebb velocity magnitudes and directions for Case RM-HR-VF (baseline), the measured data and the minimum and maximum mean values across all cases.

A. Sensitivity to flow field magnitude and direction variation

Consider now the uniform deviation of flow magnitude, $\Delta|\mathbf{u}|$ and direction, $\Delta\theta$. Fig. 3 demonstrates how modifying the flow fields for the optimisation process may alter the array layout. For any scenario, the general pattern of placement remains the same, with initial placements toward the top of the domain, followed by rows of turbines toward the bottom for wake avoidance. When the flow speed is amplified, more emphasis is placed on densely packing turbines in high energy regions. When the flow direction is rotated, more turbines are packed along the top of the domain due to the ebb direction being offset leading to less perceived wake interaction. Fig. 4 summarises the change in array power with varying flow alterations as the array is re-sited for each modified flow field (quantified on the ground truth flow fields). The base point of 0° direction change and 0 m s^{-1} velocity magnitude change corresponds to optimisation on the baseline flow fields with no artificial modification. Around this base point, small changes in direction and velocity have relatively minimal influence on the power production of the array against the baseline case. The minimal reduction in power over the range of $\pm 2^{\circ}$ aligns to a similar range in direction variation at a single point (above rated speeds) seen over a single spring-neap cycle in the flood or ebb. A large increase in velocity generally has a lesser effect than a large change in direction. Upon reaching a variation of 6° the power produced by the re-optimised array drops significantly to an average of over 5%. Arrays sited using flow fields that have been offset in both velocity magnitude and flow direction produce the worst performance, with a maximum reduction in power relative to the original optimised array of over -7.5%.

B. Sensitivity to model input changes

With different model inputs the changes to the flow fields must be considered, thus more appropriate flow instances that suited all cases were selected to steer the optimisation. Some cases had their optimisation constraint parameters altered as per Table I. Maintaining consistent optimisation constraint parameters would require fields from different instances for each input case, or alternatively using substantially more flow fields. Fig. 5 plots the change in velocity fields by

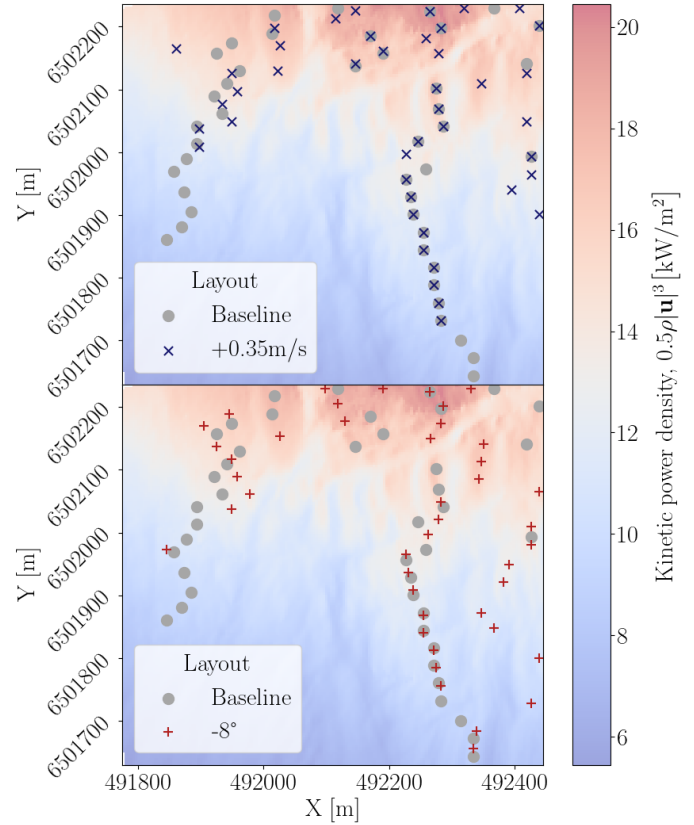


Fig. 3. Layouts of optimised arrays for artificially modified flow fields compared to the layout optimised for the ground truth flow fields. Layouts are superimposed on the average kinetic density power heatmap of the four ground truth flow fields used for optimisation.

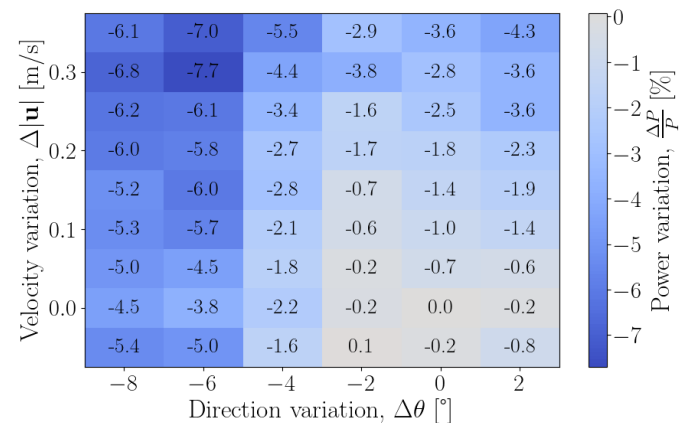


Fig. 4. Influence of artificial flow velocity errors on total array power output - showing the relative power deficit produced by an array optimised for different flow changes against the baseline flow field. Positive values correspond to uniform over-estimates.

modifying different input parameters in their expected range.

Fig. 6 indicates the relative power deficit of an array

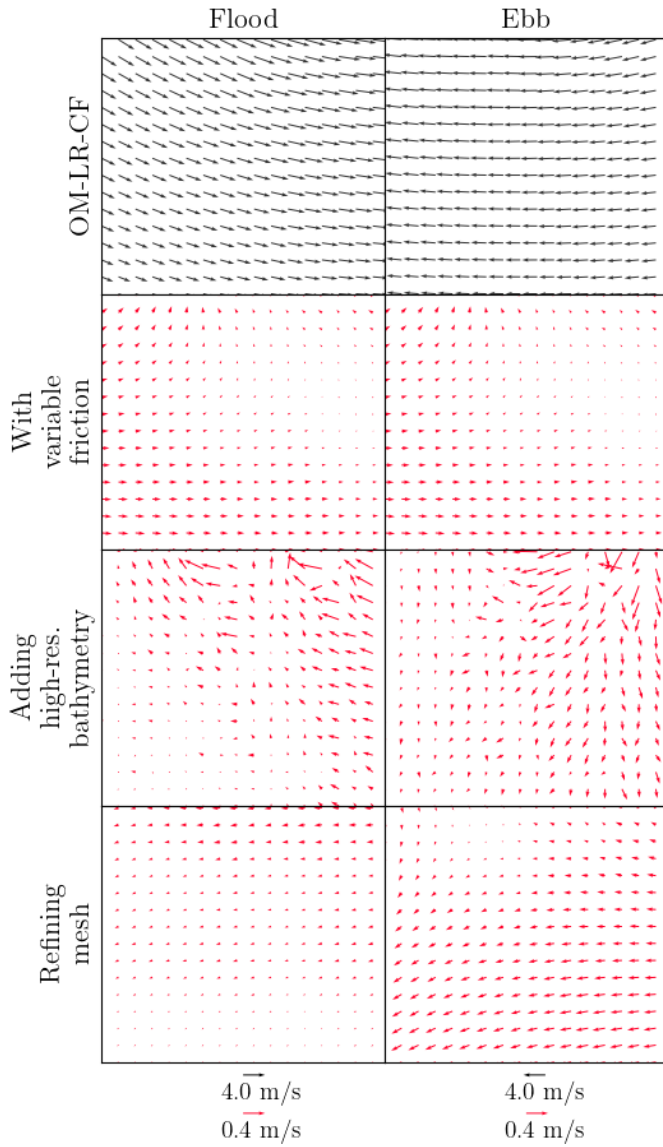


Fig. 5. Velocity field in the flood and ebb over the optimisation region for Case OM-LR-CF and the relative deficit against this case, in descending order, OM-LR-VF, OM-LR-CF, RM-LR-CF. The velocity deficit scale is $10\times$ larger than the base plot.

optimised on the case given by the x-axis against the array optimised for the quantification case given by the y-axis. Table IV shows a summary of this information by groups of optimised arrays. The most significant variation in the predicted power for an optimised array is the introduction of high-resolution bathymetry. This is followed by refinement of the mesh and then the variation in friction representation. It should be noted that when using *FLORIS* to quantify the power, based only on the four flow fields provided, the difference in relative (snapshot) power deficits are 4.55%, 1.06% and 0.39%, for bathymetry resolution, friction representation and mesh resolution respectively.

C. Sensitivity to support structure inclusion

Re-calibration of the *FLORIS* input to *Thetis* wakes with support structure inclusion had minimal influence on the far wake of an individual turbine. Support structure drag corresponds to 13.6% of modelled turbine drag at rated speeds. Thus with optimisation emphasis

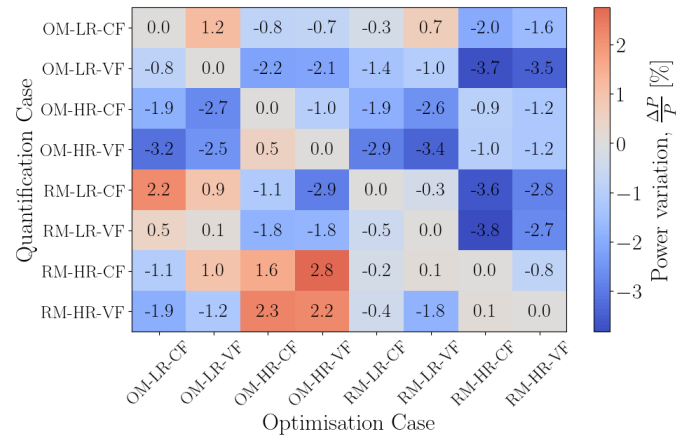


Fig. 6. Influence of input fields on total array mean power output over 10-day period - showing the relative power deficit produced by an array optimised for each case against the 'correct' case. Each column demonstrates the effectiveness of the optimised array for different input cases (relative to the 'correctly' optimised array). Each row indicates the influence on power of different optimised arrays for the same input case.

on wake avoidance and inability to consider array scale blockage, no discernable change is seen in the array layout relative to the original optimisation (excluding the effects of the support structure) based on the current model representation. Upon quantification in *Thetis*, the decrease in power to the overall array as a result of introducing the support structure was 0.23%.

IV. DISCUSSION

A. On the methodology

1) *Mesh resolution*: It should be noted that in order to take full advantage of the high-resolution bathymetry data provided the mesh would need to be further resolved. The array subdomain would extend to encompass the increased resolution data area and the mesh would be further resolved to match the data resolution. This is beyond this scope for conducting the necessary sensitivity analyses, as it would add substantial computational overhead when investigating over 100 cases.

2) *Artificial change of the flow field and choice of site*: An alternative to uniform modification of the flow field would have been to take more measurement points across the domain and to amplify the fields using an interpolation method. This would distort the fields in a non-linear fashion and alter the degree of curvature of the flow. However, this does not necessarily provide any additional insight or more accurately reflect an inaccurate estimation and would increase the difficulty in interpreting the output.

Idealised case studies could have been employed to demonstrate the sensitivity of optimisation to variations in flow direction and magnitude or directly to inputs. However, optimisation in idealised case studies such as those utilised in [7] would provide sensitivity analyses results that emanate from case design. Likewise, when investigating the sensitivity of optimisation to bathymetry or friction, the results of an idealised case could likely be easily pre-determined without running any simulations. By using a realistic case with

TABLE IV
AVERAGE RELATIVE POWER DEFICIT (%) OF GROUPS OF OPTIMISED ARRAYS FOR DIFFERENT QUANTIFICATION/CONTROL CASES.

Quantification Case	Optimisation Groups					
	Friction		Bathymetry Resolution		Mesh	
	Constant	Variable	Standard	High	Original	Refined
OM-LR-CF	-0.76	-0.13	0.39	-1.28	-0.09	-0.80
OM-LR-VF	-2.03	-1.66	-0.80	-2.88	-1.29	-2.39
OM-HR-CF	-1.17	-1.87	-2.26	-0.77	-1.39	-1.65
OM-HR-VF	-1.64	-1.78	-2.99	-0.43	-1.29	-2.13
RM-LR-CF	-0.65	-1.28	0.70	-2.63	-0.24	-1.68
RM-LR-VF	-1.40	-1.09	0.03	-2.53	-0.75	-1.75
RM-HR-CF	0.07	0.77	-0.05	0.88	1.06	-0.23
RM-HR-VF	0.02	-0.20	-1.34	1.15	0.34	-0.53
Average difference	0.46		2.14		0.94	

varying levels of data that might be encountered at different stages or array design, valuable, non-trivial insight is provided.

3) *Flow field selection*: A further issue in regard to the selection of flow fields is how this influences the emulation of over-prediction. Consider initially an adjoint-based technique where the full simulation in time is used (e.g. [3]). Amplifying the flow field speed at every timestep, the period of time over which the array is productive will be increased. The period of time over which flow speeds are between cut-in and rated would remain the same, but the time over which flow speed exceeds rated would increase. For uniform amplification or reduction of the flow speed, the ratio of time a turbine spends above rated speed to the time spent below causes a change in how efficient its position is. Higher velocity fields may mean that the array can be more densely packed, as the loss due to a wake impinging on downstream turbines during the build-up period may be less than the gain in power by spending a longer period of time above rated speed. Whilst initially intuitive, the ratio of exceeding to non-exceeding rated speeds will vary across the domain and thus emphasis on wake avoidance vs average velocity maximisation will vary spatially.

However, to reduce the computational time of iterating through hundreds of snapshots, only a few are selected here. This is a common choice where a large number of numerical simulations need to be performed or if the domain is very large. The use of representative flow fields near rated speeds, when using a limited number of snapshots, is sensible in gaining a balance between wake avoidance and high energy regions. In this case, for a few flow fields of relatively similar speeds, when the speed is uniformly amplified, the array will likely become more dense in high energy regions. However, without the temporal probability of how frequently this flow field occurs, how much denser the array becomes is not regulated. That is to say, the ratio of rated speed over- vs under-exceedance is not considered. Thus, an improvement of this study would be to utilise a number of monitoring points to apply a ratio to the power prediction in *FLORIS*, which would allow for a more accurate assessment of how important each flow field is in relation to its representative duration. This would also subsequently require an increased number of snapshots to sufficiently represent

the temporal probabilities. Nevertheless, the influence that overestimation of velocities will have in terms of changing the build-up to post-rated ratio will still be exhibited, it is just not as well moderated.

4) *Further sources of internal uncertainty not included*: Some important factors that are not discussed or explicitly considered but also contribute to the feasible power output and optimisation sensitivity are, 1) the misalignment of the tidal turbine to the flow direction, investigated and discussed in [18], 2) longer term variations in the flow as discussed in [19]. This list is not exhaustive, but serves to indicate the complex nature of the problem in practice.

B. Sensitivity to hydrodynamic model accuracy

1) *For uniform manipulation of the flow fields that guide optimisation*: Altering the model inputs has a notable impact on the velocities modelled at ADCP locations, with the R^2 value ranging from 0.777-0.979 in the flood and 0.938-0.997 in the ebb, relative to the measured data. Whilst it is expected that a 2D hydrodynamic model may overestimate velocities, some variation in correlation between modelled and measured data corresponds to the geographical features of the Inner Sound. In flood tides, a plateau emerges in low tide, thus changing the global flow pattern which may accentuate inaccuracies in the model.

As anticipated, changing the distribution and value of Manning's coefficient has a notable influence on the modelled velocity magnitudes. The variable friction representation has a higher value to the south of Stroma than the constant friction, hence the higher velocities noted at the monitoring points. The mesh did not have a substantial impact on the velocities at the ADCP monitoring points, however the global flow pattern around the island was altered, changing the perceived resource to the east of the Meygen lease area. Where the high-resolution bathymetry is available, it appears to have the most significant influence on the flow within the micro-siting area. A change in velocity magnitude was anticipated due to a difference in mean value of over 1metre between the Edina digimap and Meygen data. The increased modelled variation in local bathymetry subsequently leads to changes in direction.

By utilising the range in flood and ebb mean velocities and direction for all model and measured data, testing various 'optimised' array layouts based

on varying degree of flow field manipulations demonstrated notable optimisation sensitivity. Array layouts were generally similar in pattern, that is that placement was always based on high energy regions followed by wake avoidance leading to fences of turbines across the optimisation domain. Where velocity magnitude was overestimated, more turbines were pushed towards the higher energy regions with less focus on wake avoidance. Combining overestimated magnitude and misalignments in flow direction; within the range between modelled and measured cases; had a potential power reduction of almost 8%, relative to the ground truth case, by incorrect placement of the array. Within a range of 2° , the efficiency of the array is not reduced by more than 0.6% relative to the 'correct' direction optimisation case, until the velocity is also overestimated by 0.1m/s. A similar trend exists for velocity magnitude, with significant power drops once the overestimation of velocity exceeds 10% of the rated speed of the turbine. Upon varying the direction significantly, wake avoidance may be lost due to the misalignment between the flow fields used for optimisation and quantification, and hence within a low range of variation (within 10°) this has a more significant impact than velocity magnitude.

These trends exist whilst considering turbines with full yaw capacity, and thus the effects will be even further amplified when considering fixed direction turbines. As the velocity magnitude is increasingly overestimated, the conditions of capacity factor and neighbouring turbine losses are more easily satisfied. Hence should the velocity magnitude be underestimated, it is likely this will have a less significant impact on optimisation as long as the general flow pattern remains similar.

2) *For non-uniform changes caused by model inputs:* When comparing the performance of arrays optimised directly on flow fields from the different input cases, the inputs that have the most significant influence on the flow pattern also have the largest influence on array performance. Increasing the bathymetry resolution leads to an average of over 2% difference in average relative power deficit for arrays optimised on different input sets. Both changes to the mesh and friction also cause array average relative power deficits up to and over 0.75% between those optimised on the different representations, with the mesh having the more significant influence when quantified in *Thetis*.

There was a notable discrepancy in quantifying power in *FLORIS* and *Thetis*. Whilst *FLORIS* is treated as a black box for micro-siting, the power of each array is calculated as part of this process in a cursory manner. No slack tides are provided or proportioning factors to account for a corresponding average cycle, as there is no benefit in optimising for the slack conditions and the only requirement is to increase array power which is successfully achieved. However, from *FLORIS*' snapshot quantification, the variation of friction input was anticipated to have a more significant input than the mesh, which was reversed in the *Thetis* quantification. There are several factors that can be attributed to this. Firstly, the ratio of time spent above

rated speed relative to speeds below rated were not considered in the optimisation which may influence the effectiveness of optimisation as already discussed extensively. Secondly, hub height flow fields were used in *FLORIS* which is conservative relative to *Thetis*. This is consistent across cases, but any flow fields that were generally higher in velocity magnitude will be less influenced by the slight discrepancy between the hub height and depth-averaged flow fields by the mid- to far wake. Thirdly, the *FLORIS* version used does not model blockage effects at any scale (though local blockage can be incorporated [20]) or upstream effects due to the presence of turbines. Finally, the optimisation technique employed is still naive in its initial placement, even with the performance constraints. When an array is micro-sited using a different flow map, the highest energy regions may have different spatial distributions. Thus whilst the placement of the initial turbines may be naive for the control flow fields, it may not be for different flow fields. Hence in *Thetis*, for various reasons, some arrays optimised to the control flow fields are outperformed by others (particularly due to the greedy nature of the algorithm).

Further work could have been done in every case to find a more optimal array layout by changing or increasing the number of flow fields and further optimising the performance constraint parameters, including making them adaptive. Regardless, there is a clear, and not negligible, influence on the efficiency of the array when the inputs are changed. Irrespective of constraints, the greedy optimisation technique makes some allowance for small variation in direction by increasing the wake width using a moving average flow field and using various flow fields. Optimisation within the hydrodynamic model will also allow for some small misalignment of flow relative to the 'truth' by running the hydrodynamic quantification for long enough that there is a range of flow directions considered over time. Had the optimisation been performed within *Thetis*, friction may have had a more significant influence on array efficiency than the mesh using the adjoint, as was seen in the *FLORIS* quantification.

As the focus of this study is on optimisation, the results have been presented relative to a baseline array that has been optimised on the 'ground truth' ambient flow data. However, there is also a significant discrepancy in power prediction that should be noted. For Case RM-HR-CF, the optimised array produces an average power of 25.95MW during the quantification period. However, the same array, when quantified using the input data case RM-LR-VF produces a power of only 20.89MW. This drop of almost 20% when increasing bathymetry resolution and friction representation demonstrates how significant the input data and requirement for accurate calibration. Such a large discrepancy results from the need to recalibrate the models with more appropriate meshes or global viscosity, but there are limited ADCP and gauges to calibrate the model to, particularly for a site where the coastline changes significantly with tide level.

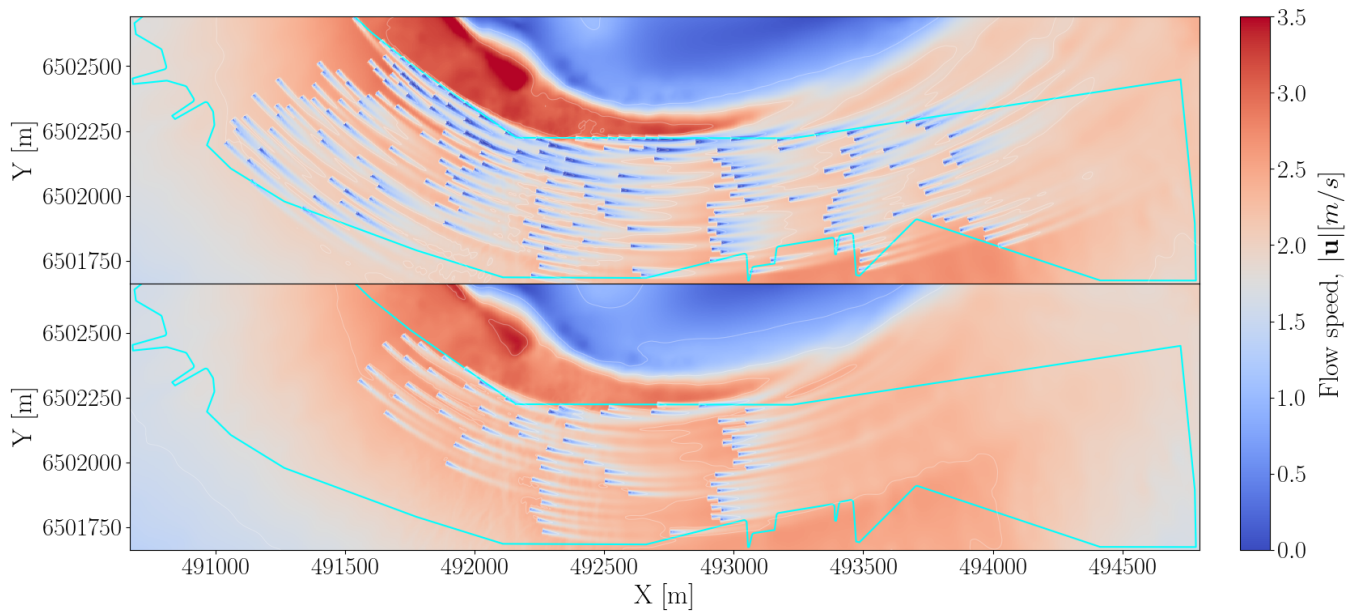


Fig. 7. Array layouts shown in *FLORIS* for a flood tide at the Meygen site with (bottom) and without (top) performance constraints included. Both cases have practical constraints applied for bathymetry depth and foundation stability. The cyan outline indicates the optimisation boundaries which are based on feasible locations.

C. Consequences of model accuracy for array developers

Focussing on just a change of bathymetry resolution, for example, there is a significant discrepancy in both the power predictions and the efficiency of the array. A change of 2% in predicted power could be the difference between a project being feasible or not. This indicates several considerations that array developers must take into account. Firstly, the proposed array, needs to be continuously re-sited when more data is made available. Secondly, the array needs to be optimised based on the full potential scale even with incremental placement, as the issues involved in not doing this are amplified by the changes in data availability as the project progresses. The scale of this is highlighted by an array micro-sited in the Meygen lease area using the same performance constraints in Fig. 7. Thirdly, bathymetry data should be collected early on in the project to avoid mis-estimation of potential power returns, as this was found to be the most significant factor on array efficiency. Finally, these uncertainties exist solely within the single model used to perform the placement. There are further variations between different models and even further variation to the actual flow as recorded by the ADCP data. Thus, array developers must consider the consequences of uncertainty that they cannot account for, not just in prediction of array power but also in terms of efficiency loss due to their array layout.

D. Support structure inclusion

The emphasis on wake avoidance in optimisation means that the inclusion of support structure did not change the array layout and had less influence on the predicted power or efficiency of the array layout than the change in input data. Placing 43 turbines in the Inner Sound does not correspond to a significant degree of global blockage as quantified in [7] and

thus the additional inclusion of support structure is unlikely to see global blockage have a large impact on power prediction. Whilst support structure is an important factor in terms of additional energy taken out of the channel, it is more pertinent to the optimisation of global array density, as opposed to sub-array scale considerations. Again, with different optimisation techniques and hydrodynamic models, more notable differences may have been produced.

V. CONCLUSIONS

The sensitivity of array optimisation at a mid-site development scale (43 turbines) was probed using artificial flow field manipulation and by variation of input data field choices. For small changes or inaccuracies in the flow field, an array will remain efficient. Overestimation of flow velocity magnitude reduces the efficiency of an array due to more dense packing of turbines due to increased exceedance of rated speed. Incorrect prediction of flow direction has a larger influence due to the emphasis of the siting algorithm on wake avoidance, whilst the combined effects of uniformly incorrect flow predictions had a reduction of almost 8% on array efficiency relative to the control optimised array layout, even for turbines with full yaw capacity. Extending to sensitivity of array layout to model input data, arrays optimised without high-resolution bathymetry data are outperformed by over 2% in average array power by arrays optimised on the new flow fields with the new bathymetry data included. The mesh resolution fineness and friction representation also caused discrepancies of up to and above 0.75% in some cases.

Site developers must therefore be mindful of the extent of uncertainty that exists, as there is a quantifiable consequence due to lack of data availability in the early stages of resource quantification. This exists

both in prediction of array power but also in terms of efficiency loss due to their array layout, which must be developed early to deal with practical constraints. Consequently, re-calibration of the model at every stage of data collection coupled with early acquisition of bathymetry and ADCP data is critical to reduce uncertainty in calculation of LCOE for site investigation and array developers.

REFERENCES

- [1] Black & Veatch, "UK Tidal Current Resource & Economics," Carbon Trust, Tech. Rep., 2011.
- [2] Z. Goss, D. Coles, and M. Piggott, "Economic analysis of tidal stream turbine arrays: a review," 2021. [Online]. Available: <https://arxiv.org/abs/2105.04718>
- [3] S. Funke, P. Farrell, and M. Piggott, "Tidal turbine array optimisation using the adjoint approach," *Renewable Energy*, vol. 63, pp. 658–673, Mar. 2014. [Online]. Available: <https://doi.org/10.1016/j.renene.2013.09.031>
- [4] D. Culley, S. Funke, S. Kramer, and P. M.D., "Integration of cost modelling within the micro-siting design optimisation of tidal turbine arrays," *Renewable Energy*, vol. 85, pp. 215–227, 2016. [Online]. Available: <https://doi.org/10.1016/j.renene.2015.06.013>
- [5] E. González-Gorbeña, R. Y. Qassim, and P. C. Rosman, "Multi-dimensional optimisation of Tidal Energy Converters array layouts considering geometric, economic and environmental constraints," *Renewable Energy*, vol. 116, pp. 647–658, 2018. [Online]. Available: <https://doi.org/10.1016/j.renene.2017.10.009>
- [6] A. Phoenix and S. Nash, "Optimisation of tidal turbine array layouts whilst limiting their hydro-environmental impact," *Journal of Ocean Engineering and Marine Energy*, vol. 5, no. 3, pp. 251–266, 2019. [Online]. Available: <https://doi.org/10.1007/s40722-019-00145-8>
- [7] C. Jordan, D. Dundovic, A. K. Fragkou, G. Deskos, D. S. Coles, M. D. Piggott, and A. Angeloudis, "Combining shallow-water and analytical wake models for tidal array micro-siting," *Journal of Ocean Engineering and Marine Energy*, vol. 8, no. 2, 3 2022.
- [8] F. Rathgeber, D. A. Ham, L. Mitchell, M. Lange, F. Luporini, A. T. T. Mcrae, G.-T. Bercea, G. R. Markall, and P. H. J. Kelly, "Firedrake: Automating the finite element method by composing abstractions," *ACM Trans. Math. Softw.*, vol. 43, no. 3, pp. 24:1–24:27, Dec. 2016. [Online]. Available: <http://doi.acm.org/10.1145/2998441>
- [9] T. Kärnä, S. C. Kramer, L. Mitchell, D. A. Ham, M. D. Piggott, and A. M. Baptista, "Thetis coastal ocean model: discontinuous galerkin discretization for the three-dimensional hydrostatic equations," *Geoscientific Model Development Discussions*, vol. 2018, pp. 1–36, 2018. [Online]. Available: <https://www.geosci-model-dev-discuss.net/gmd-2017-292/>
- [10] L. Mackie, P. S. Evans, M. J. Harrold, T. O'Doherty, M. D. Piggott, and A. Angeloudis, "Modelling an energetic tidal strait: investigating implications of common numerical configuration choices," *Applied Ocean Research*, vol. 108, no. January, p. 102494, 2021. [Online]. Available: <https://doi.org/10.1016/j.apor.2020.102494>
- [11] M. Bastankhah and F. Porté-Agel, "A new analytical model for wind-turbine wakes," *Renewable Energy*, vol. 70, pp. 116–123, 2014. [Online]. Available: <http://dx.doi.org/10.1016/j.renene.2014.01.002>
- [12] A. Niayifar and F. Porté-Agel, "Analytical modeling of wind farms: A new approach for power prediction," *Energies*, vol. 9, no. 9, pp. 1–13, 2016.
- [13] G. D. Egbert and S. Y. Erofeeva, "Efficient inverse modeling of barotropic ocean tides," *Journal of Atmospheric and Oceanic Technology*, vol. 19, no. 2, pp. 183–204, 2002. [Online]. Available: [http://dx.doi.org/10.1175/1520-0426\(2002\)019<0183:EIMOBO>2.0.CO;2](http://dx.doi.org/10.1175/1520-0426(2002)019<0183:EIMOBO>2.0.CO;2)
- [14] British Geological Society, "Seabed sediments 250k," 2020, accessed: 01-05-2023. [Online]. Available: <https://www.bgs.ac.uk/datasets/marine-sediments-250k/>
- [15] Edina Digimap Service, "Hydrospatial one, gridded bathymetry," <http://digimap.edina.ac.uk/marine/>, 2020, , SeaZone Solutions Ltd, Online; accessed 2020.
- [16] S. Muchala and R. H. Willden, "Impact of tidal turbine support structures on realizable turbine farm power," *Renewable Energy*, vol. 114, p. 588 – 599, 2017. [Online]. Available: <https://doi.org/10.1016/j.renene.2017.07.002>
- [17] R. Martin-Short, J. Hill, S. C. Kramer, A. Avdis, P. A. Allison, and M. D. Piggott, "Tidal resource extraction in the Pentland Firth, UK: Potential impacts on flow regime and sediment transport in the Inner Sound of Stroma," *Renewable Energy*, vol. 76, pp. 596–607, 2015. [Online]. Available: <http://dx.doi.org/10.1016/j.renene.2014.11.079>
- [18] C. H. Frost, P. S. Evans, M. J. Harrold, A. Mason-Jones, T. O'Doherty, and D. M. O'Doherty, "The impact of axial flow misalignment on a tidal turbine," *Renewable Energy*, vol. 113, pp. 1333–1344, 2017. [Online]. Available: <https://www.sciencedirect.com/science/article/pii/S0960148117306183>
- [19] D. Lande-Sudall, T. Stallard, and P. Stansby, "Co-located offshore wind and tidal stream turbines: Assessment of energy yield and loading," *Renewable Energy*, vol. 118, pp. 627–643, 2018. [Online]. Available: <https://www.sciencedirect.com/science/article/pii/S0960148117310248>
- [20] E. Branlard and A. R. Meyer Forsting, "Assessing the blockage effect of wind turbines and wind farms using an analytical vortex model," *Wind Energy*, vol. 23, no. 11, pp. 2068–2086, 2020.